Volume 61
Number 65
21 August 2025
Pages 12045–12220

ChemComm

Chemical Communications

rsc.li/chemcomm

ISSN 1359-7345

ROYAL SOCIETY OF CHEMISTRY

COMMUNICATION

Eduard Y. Chekmenev, Thomas Theis *et al.*

SABRE-SHEATH hyperpolarized $^{15}N_2$-imidazole for Zn^{2+} sensing

ChemComm

COMMUNICATION

View Article Online
View Journal | View Issue

Cite this: *Chem. Commun.*, 2025, **61**, 12115

Received 22nd May 2025,
Accepted 19th June 2025

DOI: 10.1039/d5cc02890f

rsc.li/chemcomm

SABRE-SHEATH hyperpolarized $^{15}N_2$-imidazole for Zn^{2+} sensing†

Brojo Kishor Shachib Dhali, ‡[a] Abubakar Abdurraheem, ‡[b] Mustapha Abdulmojeed,[a] Anna Samoilenko,[b] Megan Pike,[a] Rielly J. Harrison,[a] Franziska Theiss,[a] Boyd M. Goodson,[c] Eduard Y. Chekmenev *[b] and Thomas Theis *[a]

Zinc ions are essential for numerous biological functions and activities. Accordingly, Zn^{2+} sensors are crucial in biomedical research to understand the role of Zn^{2+} in health and disease. Here, we demonstrated the viability of SABRE-SHEATH hyperpolarized $^{15}N_2$-imidazole, providing an NMR signal enhancement of 45 700 fold (p = 2.15%), as a probe for Zn^{2+} sensing by monitoring the Zn-imidazole interaction using NMR and extracted a LOD of 1.3 mM. This study is one of the first demonstrations of SABRE-SHEATH hyperpolarized ^{15}N as a sensor of other non-hyperpolarized species, which promises chemical sensing without penetration-depth limitations.

Nuclear Magnetic Resonance (NMR) is a powerful technique for non-destructive structural elucidation and monitoring of molecular interactions. However, NMR is notoriously insensitive, especially for heteronuclei, such as ^{13}C and ^{15}N, and requires large sample volumes or high concentrations. Therefore, the study of low-concentration targets often remains out of reach.[1,2] In this work, we employed Signal Amplification By Reversible Exchange in SHield Enables Alignment Transfer to Heteronuclei (SABRE-SHEATH), to enhance the ^{15}N NMR signal of $^{15}N_2$-imidazole up to ~45 700 fold at 1.4 T (p = 2.15%). The hyperpolarized $^{15}N_2$-imidazole is subsequently used to quantify the Zn^{2+} content in a test solution *via* changes of the ^{15}N chemical shift upon $^{15}N_2$-imidazole binding to Zn^{2+}.

SABRE-SHEATH is a cost-effective and non-destructive hyperpolarization technique. SABRE-SHEATH creates nuclear spin polarization of a target molecule by simultaneous chemical exchange of *para*hydrogen (p-H_2) and the target on an iridium catalyst.[3–15] The employed pre-catalyst is [IrCl(COD)(IMes)] (where, IMes = 1,3-bis(2,4,6-trimethyl-phenyl)imidazole-2-ylidene), which forms the active polarization transfer catalyst as illustrated in Fig. 1. The afforded signal enhancement is subsequently used to monitor the interaction between the ^{15}N nuclei of $^{15}N_2$-imidazole and Zn^{2+}.

Zinc is a crucial trace element with different biological activities, including enzyme catalysis, gene expression, cell signaling, and immune response.[16–23] Zinc ions also regulate neuronal activity and synaptic plasticity in the brain.[24–28] Accordingly, Zn^{2+} sensors play vital roles in biomedical research used to detect and monitor Zn^{2+} ions in biological systems. Understanding the physiological and pathological roles of Zn^{2+} ions in various biological functions and diseases is critical to the development of new diagnostic and therapeutic strategies.[29–33] Literature demonstrates that Zn^{2+} ions interact with the nitrogen atoms of imidazole to form coordination complexes with coordination numbers of one, two, three, or four—predominantly four.[34–38] The present study showcases the ability of hyperpolarized $^{15}N_2$-imidazole to detect Zn^{2+}. We selected this system because of imidazole's ability to coordinate with Zn^{2+}, and the diamagnetic nature of Zn^{2+}, which avoids

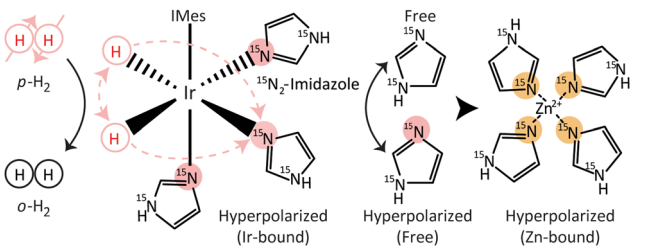

Fig. 1 Illustration of the reversible exchange of p-H_2 and $^{15}N_2$-imidazole on the iridium catalyst promoting polarization transfer through a J-coupling network. Initially, p-H_2 transfers its spin order to catalyst-bound $^{15}N_2$-imidazole, which subsequently exchanges off the catalyst to form free, hyperpolarized $^{15}N_2$-imidazole. Finally, the hyperpolarized $^{15}N_2$-imidazole binds to Zn^{2+}. The hyperpolarized $^{15}N_2$-imidazole NMR signal directly reports on the binding event.

[a] *Department of Chemistry, North Carolina State University, Raleigh, North Carolina, 27965-8204, USA. E-mail: bdhali@ncsu.edu, ttheis@ncsu.edu*
[b] *Department of Chemistry, Karmanos Cancer Institute, Wayne State University, Detroit, MI, 8202, USA. E-mail: gq3501@wayne.edu*
[c] *School of Chemical & Biomolecular Sciences, Southern Illinois University, Carbondale, Illinois 62901, USA*

† Electronic supplementary information (ESI) available. See DOI: https://doi.org/10.1039/d5cc02890f

‡ Contributed equally to the experiments.

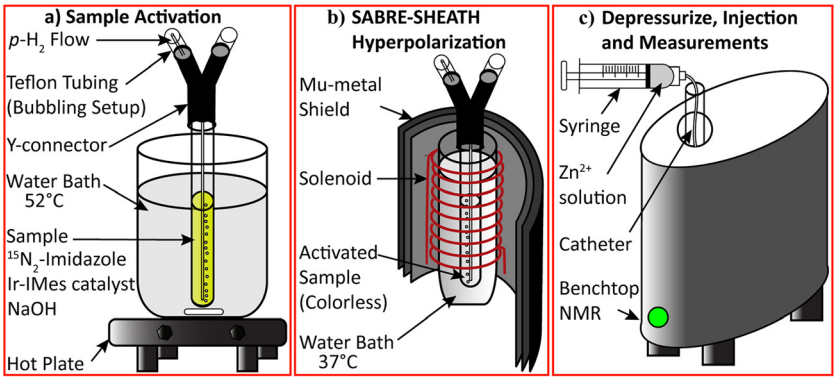

Fig. 2 Schematic diagram depicting the process of Zn^{2+} sensing using hyperpolarized $^{15}N_2$-imidazole. (a) The sample was activated by bubbling p-H_2 while it was in a heated water bath. (b) The activated sample was hyperpolarized in the mu-metal shield by bubbling p-H_2 at an optimized polarization transfer field. (c) The hyperpolarized solution was transferred to the benchtop NMR, depressurized, and the target (Zn^{2+}) was injected.

paramagnetic relaxation of the hyperpolarized ^{15}N nuclear spins.[34,39]

Previous work showed that $^{15}N_2$-imidazole hyperpolarizes more effectively under basic conditions.[40] Therefore, a sample containing 100 mM $^{15}N_2$-imidazole, 6 mM Ir-IMes pre-catalyst and 1 mM NaOH in methanol was prepared, and a 0.8 mL aliquot of the solution was carefully transferred into an NMR tube, as shown in Fig. 2. The hyperpolarization pre-catalyst in the sample was then activated by flowing p-H_2 at a rate of 100 sccm and a pressure of 100 psi at 52 °C for 10 minutes. Once fully activated, the sample changed color from pale yellow to colorless. The activated sample was transferred to a mu-metal shield, where p-H_2 was bubbled for 40 seconds at an optimized polarization transfer field of 0.4 μT and a temperature of 37 °C to hyperpolarize the ^{15}N nuclei of $^{15}N_2$-imidazole (see ESI,† Section S8 for the optimization studies of polarization build-up, polarization transfer field and temperature). After hyperpolarization, the sample was transferred to a 1.4 T Magritek benchtop NMR spectrometer and depressurized by disconnecting the NMR sample tube from the bubbling setup. Immediately, a 30-degree pulse was applied to acquire a proton-decoupled ^{15}N NMR signal of neutral $^{15}N_2$-imidazole. Finally, the analyte of interest (Zn^{2+} solution, or HCl solution, or methanol for the control experiment) was injected into the NMR tube using a syringe. The solutions were mixed by shaking the PTFE catheter, and a 30-degree pulse was applied to acquire the proton-decoupled ^{15}N NMR signal to detect the chemical interactions (see ESI,† Section S2 for detailed experimental procedure and data processing).

The primary objective of this study was to quantify the Zn^{2+} content in a test solution *via* changes of the ^{15}N chemical shift upon $^{15}N_2$-imidazole binding to Zn^{2+}. Previous work showed that hyperpolarized $^{15}N_2$-imidazole can be used as a pH probe.[40] Because the analyte of interest, $ZnCl_2$, is slightly acidic,[40–42] the ^{15}N chemical shift of imidazole may not only respond to zinc binding but also to changes in pH. Therefore, it was necessary to distinguish pH-induced shifts from binding-induced shifts. To test the pH effect in isolation, we titrated the hyperpolarized $^{15}N_2$-imidazole with a strong acid (HCl) to identify a range where $^{15}N_2$-imidazole remains in its original form (neutral structure) and its peak position remains unchanged. As illustrated in Fig. 3, the neutral structure of $^{15}N_2$-imidazole displayed identical chemical shifts (203.4 ppm) for both ^{15}N nuclei as a result of rapid proton hopping between the two nitrogen sites. Imidazole reacts as a weak base, and adopts a protonated structure in an acidic environment, resulting in a decrease in ^{15}N NMR frequency below pH ≈ 6.2. Note that in these ^{15}N spectra, no ^{1}H splitting was observed because the spectra were proton-decoupled (see ESI,† Fig. S1, for a spectrum over a larger bandwidth). The additional minor peaks in the ^{15}N spectra correspond to the Ir-bound $^{15}N_2$-imidazole species at various positions within the $^{15}N_2$-imidazole hexacoordinate Ir complex. The exact spectral assignment of the

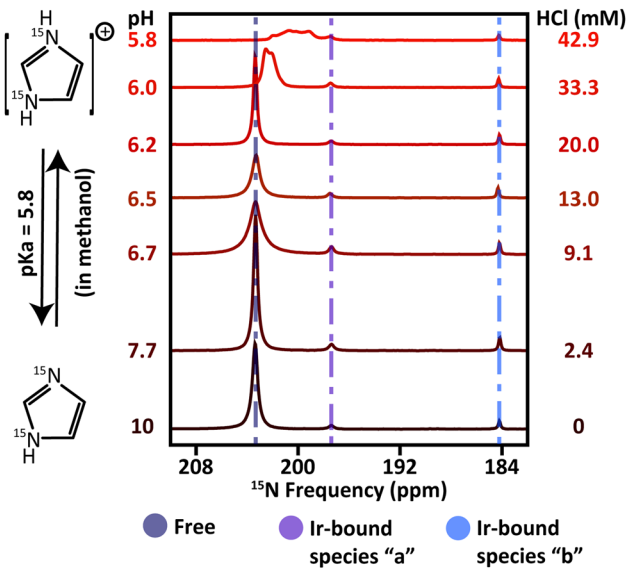

Fig. 3 Titration of $^{15}N_2$-imidazole with HCl. No shift in peak position was observed up to a concentration of 20 mM HCl, with sensitivity beginning below a pH of ≈6.2. Species "a" and "b" represent unidentified Ir-bound $^{15}N_2$-imidazole at two different positions within the $^{15}N_2$-imidazole hexacoordinate Ir complex. The HCl (mM) column represents the HCl concentration in the mixture, whereas the pH column reports the pH of the final mixture (see ESI,† Section S6 for more information on pH and Fig. S4 for the measurement of the pK_a value of $^{15}N_2$-imidazole in methanol, ESI†).

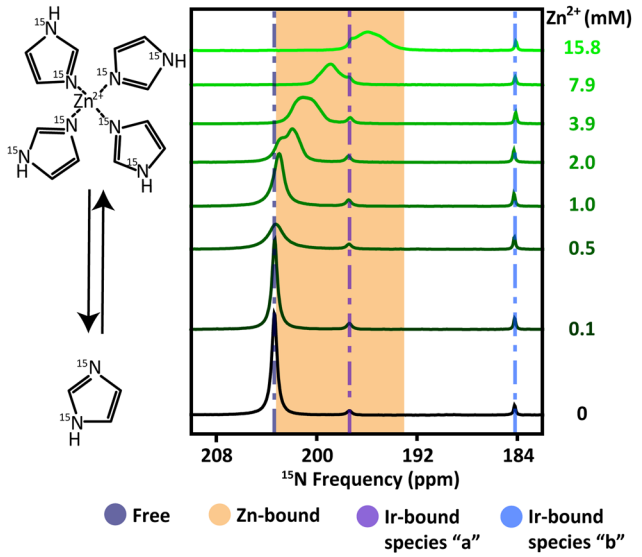

Fig. 4 The response of $^{15}N_2$-imidazole chemical shift to the addition of Zn^{2+}. The frequency of $^{15}N_2$-imidazole is reduced as Zn^{2+} is added gradually, indicating the formation of Zn-bound $^{15}N_2$-imidazole complexes. Species "a" and "b" represent unidentified Ir-bound $^{15}N_2$-imidazole at two different positions within the $^{15}N_2$-imidazole hexacoordinate Ir complex. The Zn^{2+} (mM) column represents the final Zn^{2+} concentration in the mixture.

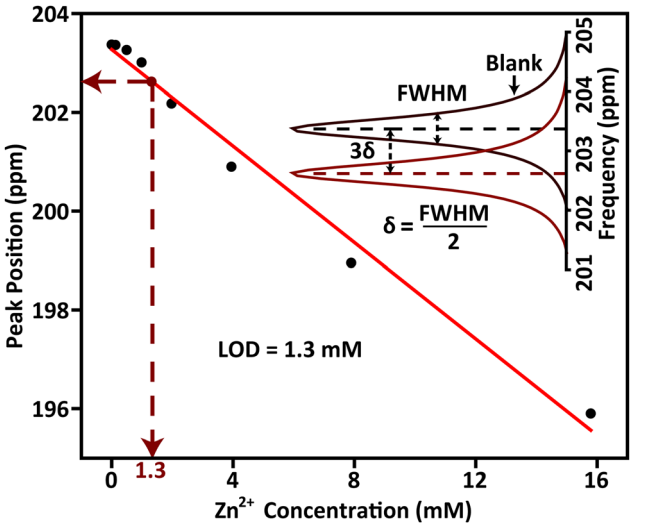

Fig. 5 Calibration curve for Zn^{2+} sensing with hyperpolarized $^{15}N_2$-imidazole. A linear correlation between the $^{15}N_2$-imidazole peak shift and Zn^{2+} concentration is identified (R^2 = 0.984). LOD estimation is depicted, with the blank measurement (black) separated from the subsequent measurement (brown) by 3δ, yielding a LOD value of 1.3 mM.

bound ^{15}N peaks remains ambiguous at this time (see ESI,† Section S3 for further discussion). In the titration study with HCl, we found that the main (free) ^{15}N peak position remained stable up to a concentration of 20 mM HCl (pH $\approx$ 6.2) as shown in Fig. 3. Since HCl is highly acidic compared to $ZnCl_2$, this finding gave us confidence to add $ZnCl_2$ up to 20 mM in our sample and attribute any chemical shift changes to binding between Zn^{2+} ions and $^{15}N_2$-imidazole.

We then proceeded with Zn^{2+} sensing by adding $ZnCl_2$ solution up to 15.8 mM into our hyperpolarized $^{15}N_2$-imidazole sample and acquiring ^{15}N NMR spectra to observe chemical shift changes, as illustrated in Fig. 4. The pH of the sample mixture was recorded as $\approx$7.3 after adding $ZnCl_2$ to a final concentration of 15.8 mM and was well within the region where peak position remains unchanged due to pH (see Fig. 3). Therefore, any observed shifts can be attributed exclusively to Zn^{2+} binding. The ^{15}N NMR spectrum of hyperpolarized $^{15}N_2$-imidazole before and after the addition of $ZnCl_2$ solution clearly indicated a reduction in chemical shift, confirming the interaction between Zn^{2+} ions and $^{15}N_2$-imidazole, as shown in Fig. 4. In addition to a chemical shift change, line broadening is observed at higher Zn^{2+} concentrations, which can be attributed to ligand exchange on Zn^{2+}. Upon Zn^{2+} binding, the chemical equivalence of the two ^{15}N sites in $^{15}N_2$-imidazole is broken, which also contributes to the observed broadening in addition to exchange. Although the line broadening effect could also be used to quantify Zn^{2+} binding, the change in chemical shift is a more reliable measure to quantify Zn^{2+} concentration, which we quantified with the calibration curve presented in Fig. 5.

The calibration curve shown in Fig. 5 revealed a linear dependence of peak shift with Zn^{2+} concentration. To obtain the depicted calibration curve, peak positions were identified as the center of the Full Width at Half Maximum (FWHM), as opposed to choosing the location of highest intensity in the spectrum. Using the depicted calibration curve, we proceeded to determine the Limit of Detection (LOD) for Zn^{2+} sensing with hyperpolarized $^{15}N_2$-imidazole. LOD is calculated as $((y_b - c) - 3\delta)/m$, where y_b = blank measurement (peak position of free $^{15}N_2$-imidazole without addition of Zn^{2+}), c = intercept of the calibration curve, m = slope of the calibration curve, and δ represents the standard deviation of the blank measurements.[43–45] In this method, the FWHM serves as the most direct measure of uncertainty, as it defines the minimum chemical shift difference required to distinguish two peaks. Therefore, we set δ = FWHM/2 of the NMR line of blank measurement. This concept is illustrated in Fig. 5, showing the blank measurement (black) separated from the subsequent measurement (brown) by 3δ, which allows for distinction of the peaks and thus determines the LOD. As a result, the LOD was determined as 1.3 mM for Zn^{2+} using hyperpolarized $^{15}N_2$-imidazole as the sensor (see ESI,† Section S7 for full calculation).

In conclusion, we introduced ^{15}N hyperpolarized tracers as biochemical sensors for indirect sensing of a non-hyperpolarized species. Specifically, the interaction between hyperpolarized $^{15}N_2$-imidazole with Zn^{2+} was shown using a 1.4 T Magritek benchtop NMR spectrometer. To this end, we first isolated peak shifts due to pH changes from peak shifts due to Zn^{2+} binding by carefully characterizing the system's behavior in the pH range of 10 to 5.8. Subsequently, we observed the changes in the ^{15}N NMR spectra as a function of added $ZnCl_2$ solution and found a significant response of the peak position and the line broadening. The peak position was used to establish a calibration curve for Zn^{2+} sensing with hyperpolarized $^{15}N_2$-imidazole. From the calibration curve, a

LOD of 1.3 mM was extracted. This work demonstrates the use of hyperpolarized ^{15}N probes as molecular sensors, exemplified by $^{15}N_2$-imidazole as a probe for Zn^{2+} sensing. For future physiological applications, it will be crucial to enhance the Zn^{2+} sensor's sensitivity to the micromolar-to-nanomolar range, for example, *via* decreasing the concentration of hyperpolarized $^{15}N_2$-imidazole in the sample. Furthermore, ensuring biocompatibility by eliminating methanol as a solvent is essential. Possible strategies to achieve this include phase separation or gas stripping.[46,47] The emerging technology is positioned to probe the role of Zn^{2+} or other ions and their biological activities, such as enzyme catalysis, gene expression, or cell signaling.

This material is based upon work supported by the U.S. Department of Energy, Office of Biological and Environmental Research (BER) under award number(s) DE-SC0023334 and DE-SC0025315 (TT & EYC). Funding of this work was also provided by the NIH under R21EB033872 (EYC & BMG), and NSF grants CHE-2404387 (BMG) and CHE-2404388 (EYC). This report was prepared as an account of work sponsored by an agency of the United States Government. The views and opinions of authors expressed herein do not necessarily state or reflect those of the United States Government or any agency.

Conflicts of interest

E. Y. C. and B. M. G. are co-founders and equity holders of XeUS Technologies LTD.

Data availability

The data supporting this article have been included as part of the ESI.†

References

1 M.-C. Malet-Martino and R. Martino, *Clin. Pharmacokinet.*, 1991, **20**, 337–349.
2 M. V. S. Elipe, *Anal. Chim. Acta*, 2003, **497**, 1–25.
3 R. W. Adams, J. A. Aguilar, K. D. Atkinson, M. J. Cowley, P. I. Elliott, S. B. Duckett, G. G. Green, I. G. Khazal, J. López-Serrano and D. C. Williamson, *Science*, 2009, **323**, 1708–1711.
4 T. Theis, M. L. Truong, A. M. Coffey, R. V. Shchepin, K. W. Waddell, F. Shi, B. M. Goodson, W. S. Warren and E. Y. Chekmenev, *J. Am. Chem. Soc.*, 2015, **137**, 1404–1407.
5 P. TomHon, M. Abdulmojeed, I. Adelabu, S. Nantogma, M. S. H. Kabir, S. Lehmkuhl, E. Y. Chekmenev and T. Theis, *J. Am. Chem. Soc.*, 2021, **144**, 282–287.
6 K. MacCulloch, A. Browning, P. TomHon, S. Lehmkuhl, E. Y. Chekmenev and T. Theis, *Anal. Chem.*, 2023, **95**, 7822–7829.
7 I. M. Senanayake, M. S. Alam, M. S. Kabir, A. F. Petrilla, Z. Siraj, T. Theis, E. Y. Chekmenev and B. M. Goodson, *J. Phys. Chem. B*, 2025, **129**(5), 1662–1669.
8 K. MacCulloch, A. Browning, D. O. G. Bedoya, S. J. McBride, M. B. Abdulmojeed, C. Dedesma, B. M. Goodson, M. S. Rosen, E. Y. Chekmenev, Y.-F. Yen, P. TomHon and T. Theis, *J. Magn. Reson. Open*, 2023, **16**, 100129.
9 M. L. Truong, T. Theis, A. M. Coffey, R. V. Shchepin, K. W. Waddell, F. Shi, B. M. Goodson, W. S. Warren and E. Y. Chekmenev, *J. Phys. Chem. C*, 2015, **119**, 8786–8797.
10 T. Theis, M. Truong, A. M. Coffey, E. Y. Chekmenev and W. S. Warren, *J. Magn. Reson.*, 2014, **248**, 23–26.
11 D. A. Barskiy, R. V. Shchepin, A. M. Coffey, T. Theis, W. S. Warren, B. M. Goodson and E. Y. Chekmenev, *J. Am. Chem. Soc.*, 2016, **138**, 8080–8083.
12 J. F. Colell, A. W. Logan, Z. Zhou, R. V. Shchepin, D. A. Barskiy, G. X. Ortiz Jr, Q. Wang, S. J. Malcolmson, E. Y. Chekmenev, W. S. Warren and T. Theis, *J. Phys. Chem. C*, 2017, **121**, 6626–6634.
13 P. Nikolaou, B. M. Goodson and E. Y. Chekmenev, *Chem. – Eur. J.*, 2015, **21**, 3156–3166.
14 J. B. Hövener, A. N. Pravdivtsev, B. Kidd, C. R. Bowers, S. Glöggler, K. V. Kovtunov, M. Plaumann, R. Katz-Brull, K. Buckenmaier, A. Jerschow, F. Reineri, T. Theis, R. V. Shchepin, S. Wagner, P. Bhattacharya, N. M. Zacharias and E. Y. Chekmenev, *Angew. Chem., Int. Ed.*, 2018, **57**, 11140–11162.
15 K. V. Kovtunov, E. V. Pokochueva, O. G. Salnikov, S. F. Cousin, D. Kurzbach, B. Vuichoud, S. Jannin, E. Y. Chekmenev, B. M. Goodson, D. A. Barskiy and I. V. Koptyug, *Chem. – Asian J.*, 2018, **13**, 1857–1871.
16 M. Stefanidou, C. Maravelias, A. Dona and C. Spiliopoulou, *Arch. Toxicol.*, 2006, **80**, 1–9.
17 R. Patil, T. Sontakke, A. Biradar and D. Nalage, *Food Health*, 2023, **5**, 13.
18 H. Tapiero and K. D. Tew, *Biomed. Pharmacother.*, 2003, **57**, 399–411.
19 F. S. Al-Fartusie and S. N. Mohssan, *Indian J. Adv. Chem. Sci.*, 2017, **5**, 127–136.
20 W. Mertz, *Science*, 1981, **213**, 1332–1338.
21 W. Maret, *Adv. Nutr.*, 2013, **4**, 82–91.
22 B. Vallee and K. Falchuk, *Philos. Trans. R. Soc., B*, 1981, **294**, 185–197.
23 W. Maret, *Int. J. Mol. Sci.*, 2017, **18**, 2285.
24 E. P. Huang, *Proc. Natl. Acad. Sci. U. S. A.*, 1997, **94**, 13386–13387.
25 A. S. Nakashima and R. H. Dyck, *Brain Res. Rev.*, 2009, **59**, 347–373.
26 M. Mayer and L. Vyklicky Jr, *J. Physiol.*, 1989, **415**, 351–365.
27 X. Xie and T. G. Smart, *Nature*, 1991, **349**, 521–524.
28 P. Paoletti, A. Vergnano, B. Barbour and M. Casado, *Neuroscience*, 2009, **158**, 126–136.
29 S. A. Dabravolski, N. K. Sadykhov, A. G. Kartuesov, E. E. Borisov, V. N. Sukhorukov and A. N. Orekhov, *Int. J. Mol. Sci.*, 2022, **23**, 6890.
30 T. Mazur, M. Malik and D. C. Bieńko, *J. Inorg. Biochem.*, 2024, 112601.
31 E. Leclerc and C. W. Heizmann, *Front. Biosci., Scholar Ed.*, 2011, **3**, 1232–1262.
32 J. M. Rozenberg, M. Kamynina, M. Sorokin, M. Zolotovskaia, E. Koroleva, K. Kremenchutckaya, A. Gudkov, A. Buzdin and N. Borisov, *Biomedicines*, 2022, **10**, 1072.
33 B. Turan and E. Tuncay, *Int. J. Mol. Sci.*, 2017, **18**, 2395.
34 A. Lagutschenkov, U. J. Lorenz and O. Dopfer, *Int. J. Mass Spectrom.*, 2011, **308**, 316–329.
35 D. W. Appleton and B. Sarkar, *Bioinorg. Chem.*, 1977, **7**, 211–224.
36 M. Tašner, D. Vušak, I. Kekez, A. Gabud, V. Pilepić, D. Mrvoš-Sermek and D. Matković-Čalogović, *Heliyon*, 2022, **8**, e11100.
37 K. G. Anjali, K. V. Jibin, P. V. Aswathy, A. A. Shanty, F. Shijo, T. M. Dhanya, D. P. Savitha and P. V. Mohanan, *J. Photochem. Photobiol., A*, 2022, **433**, 114134.
38 M. Andersson, J. Hedin, P. Johansson, J. Nordström and M. Nydén, *J. Phys. Chem. A*, 2010, **114**, 13146–13153.
39 A. Upadhyay, C. Das, S. Vaidya, S. K. Singh, T. Gupta, R. Mondol, S. K. Langley, K. S. Murray, G. Rajaraman and M. Shanmugam, *Chem. – Eur. J.*, 2017, **23**, 4903–4916.
40 R. V. Shchepin, D. A. Barskiy, A. M. Coffey, T. Theis, F. Shi, W. S. Warren, B. M. Goodson and E. Y. Chekmenev, *ACS Sens.*, 2016, **1**, 640–644.
41 S. Kobayashi, T. Busujima and S. Nagayama, *Chem. – Eur. J.*, 2000, **6**, 3491–3494.
42 J. Sun, L. Wang, S. Zhang, Z. Li, X. Zhang, W. Dai and R. Mori, *J. Mol. Catal. A: Chem.*, 2006, **256**, 295–300.
43 G. L. Long and J. D. Winefordner, *Anal. Chem.*, 1983, **55**, 712A–724A.
44 D. A. Armbruster and T. Pry, *Clin. Biochem. Rev.*, 2008, **29**(1), S49–S52.
45 Y. Li, X. Zhang, B. Zhu, J. Yan and W. Xu, *Anal. Sci.*, 2010, **26**, 1077–1080.
46 S. Petersen, L. Nagel, P. R. Groß, H. de Maissin, R. Willing, L. Heß, J. Mitschke, N. Klemm, J. Treiber, C. A. Müller, S. Knecht, I. Schwartz, M. Weigt, M. Bock, D. von Elverfeldt, M. Zaitsev, E. Y. Chekmenev, J.-B. Hövener, A. F. Martins, F. Schilling, T. Reinheckel and A. B. Schmidt, *Theranostics*, 2025, **15**, 3714.
47 S. J. McBride, M. Pike, E. Curran, A. Zavriyev, B. Adebesin, L. Tucker, J. M. Harzan, I. M. Senanayake, S. Shen, M. Abdulmojeed, F. Theiss, T. Boele, T. P. Gade, S. Duckett, B. M. Goodson, M. S. Rosen, E. Y. Chekmenev, H. Yuan, C. Dedesma, S. Kadlecek, T. Theis and P. TomHon, *Angew. Chem., Int. Ed.*, 2025, e202501231.

